Title: Recent odor experience selectively modulates olfactory sensitivity across the glomerular output in the mouse olfactory bulb

Abbreviated Title: Selective adaptation in olfactory bulb output

Authors: Narayan Subramanian[1], Lee Min Leong[1], Paria Salemi Mokri Boukani[1,2], Douglas A. Storace[1*,2,3]
[1]Department of Biological Science, Florida State University, Tallahassee, FL
[2]Program in Neuroscience, Florida State University, Tallahassee, FL
[3]Institute of Molecular Biophysics, Florida State University, Tallahassee, FL

*** Corresponding Author**:
Douglas A. Storace
107 Chieftan Way
Biomedical Research Facility
Department of Biological Science
Program in Neuroscience
Institute of Molecular Biophysics
Florida State University
Tallahassee, FL 32306
dstorace@fsu.edu
Number of pages: 23
Number of figures: 9
Abstract word count: 250
Introduction word count: 618
Discussion word count: 1473

ORCID Numbers: (D. Storace) = https://orcid.org/0000-0002-3535-5472

Conflict of interest: The authors declare no competing financial interests.

Keywords: Olfactory bulb; Optical imaging; 2-photon, calcium imaging; adaptation; mouse

Abstract: Although animals can reliably locate and recognize odorants embedded in complex environments, the neural circuits for accomplishing these tasks remain incompletely understood. Adaptation is likely to be important in this process as it could allow neurons in a brain area to adjust to the broader sensory environment. Adaptive processes must be flexible enough to allow the brain to make dynamic adjustments, while also maintaining sufficient stability such that organisms do not forget important olfactory associations. Processing within the mouse olfactory bulb is likely involved in generating adaptation, although there are conflicting models of how it transforms the glomerular output of the mouse olfactory bulb. Here we performed 2-photon Ca^{2+} imaging in awake mice to determine the time course of recovery from adaptation, and whether it acts broadly or selectively acts across the glomerular population. Individual glomerular responses, as well as the overall population odor representation was similar across imaging sessions. However, odor-concentration pairings presented with interstimulus intervals upwards of 30-s could evoke heterogeneous adaptation across the glomerular population. This adaptation was strongest at higher concentrations, unrelated to variations in respiration, and measurements from olfactory receptor neuron glomeruli indicate that it is unlikely to be inherited from the periphery. Our results indicate that the olfactory bulb output reliably transmits stable odor representations, although dynamic processes exist by which recent odor exposure can selectively impact odor sensitivity for upwards of 30 seconds. We propose that dynamic adaptation in subsets of glomeruli is necessary for making dynamic adjustments to complex odor environments.

69 **Introduction.**

70 Although animals can reliably locate and recognize odorants embedded in complex chemical
71 contexts, the neural circuits for accomplishing these tasks remain incompletely understood [1-3]. The
72 ability to attend to, and segment different kinds of odorant information would be facilitated by adaptive
73 processes within the brain that could adjust responsiveness based on an organism's sensory
74 environment and internal state [4-8]. Such adaptive processes should be flexible enough to allow the
75 brain to make dynamic adjustments to different sensory environments, while also maintaining
76 sufficient stability such that organisms do not forget important olfactory associations. Defining the
77 brain areas and understanding how adaptation transforms olfactory representations remains an area
78 of strong interest within the neuroscience community [9-11].

79 Odors evoke varying degrees of neural activity across the olfactory receptor neuron
80 population, yielding a combinatorial code that is transmitted to the olfactory bulb [12-17]. Each
81 olfactory receptor type typically maps to one or two regions of neuropil called glomeruli in the
82 olfactory bulb [18, 19]. Mitral and tufted cells each innervate a single glomerulus where they receive
83 olfactory receptor input, and send a transformed sensory representation to the rest of the brain [15,
84 20-22]. Recent work has shown that processing within the mouse olfactory bulb is involved in
85 generating adaptation in the glomerular output of the mouse olfactory bulb [22]. However, there are
86 conflicting models of how adaptation impacts the transmission of olfactory sensory information from
87 the bulb to the rest of the brain. There currently exists data to support the presence of adaptation that
88 occurs gradually over days and broadly impacts the output of the bulb, as well as adaptation that is
89 shorter-lasting and selective in which glomerular output channels are affected [22-25].

90 We tested these models using *in vivo* 2-photon Ca^{2+} imaging from the apical dendrites of
91 mitral/tufted cells innervating the olfactory bulb glomerular layer in awake mice. A panel of odors at
92 different concentrations were delivered at different interstimulus intervals on the same day, or during
93 imaging sessions performed on different days. Odor representations across the mitral/tufted
94 glomerular population had similar amplitudes and were well correlated across trials taken on the

same day separated by a minimum of 3 minutes, and in trials on different imaging days. However, adaptation was present in response to odors delivered with a 6-s interstimulus interval that was highly selective across the mitral/tufted glomerular population. Within the same imaging field of view, some glomeruli responded similarly to each odor presentation, while others changed significantly. This adaptation was strongly concentration-dependent with higher concentrations evoking significantly more adaptation across the glomerular population. Extending the interstimulus interval to 30-s resulted in an incomplete recovery from adaptation. Measurements of animal respiration and odor-evoked activity in olfactory receptor neuron glomeruli suggest that adaptation is unlikely to reflect variations in the organismal state or sensory input. Our results indicate that the mouse olfactory bulb transmits reliable representations of olfactory stimuli across time, although there exist neural processes that can selectively mediate sensitivity adjustments based on recent odor exposure for upwards of 30 seconds. We propose that dynamic adaptation in subsets of glomeruli would be useful for making dynamic adjustments to complex odor environments [9].

Results

Odors evoke similar responses in mitral/tufted glomeruli when measured during the same imaging session or across different days.

To selectively image from mitral/tufted glomeruli, the Tbx21-Cre transgenic mouse line (that expresses cre recombinase in mitral/tufted cells) was mated to the Ai148 cre-dependent GCaMP6f reporter line [26, 27]. The resulting transgenic offspring that expressed both genes were confirmed to express GCaMP6f in mitral/tufted cells in the mouse olfactory bulb in histological sections (**Fig 1A**). During *in vivo* imaging in awake mice, mitral/tufted glomeruli were clearly visible in the *in vivo* mean fluorescence, and odors evoked activity in different glomeruli within the field of view (**Fig 1B**, *day 1*). The strong and stable GCaMP6f expression levels allowed for routine imaging from the glomerular layer using moderate laser power (< 150 mW) in thinned skull preparations as well as cranial window preparations. The results from both kinds of preparations were not qualitatively different from one another.

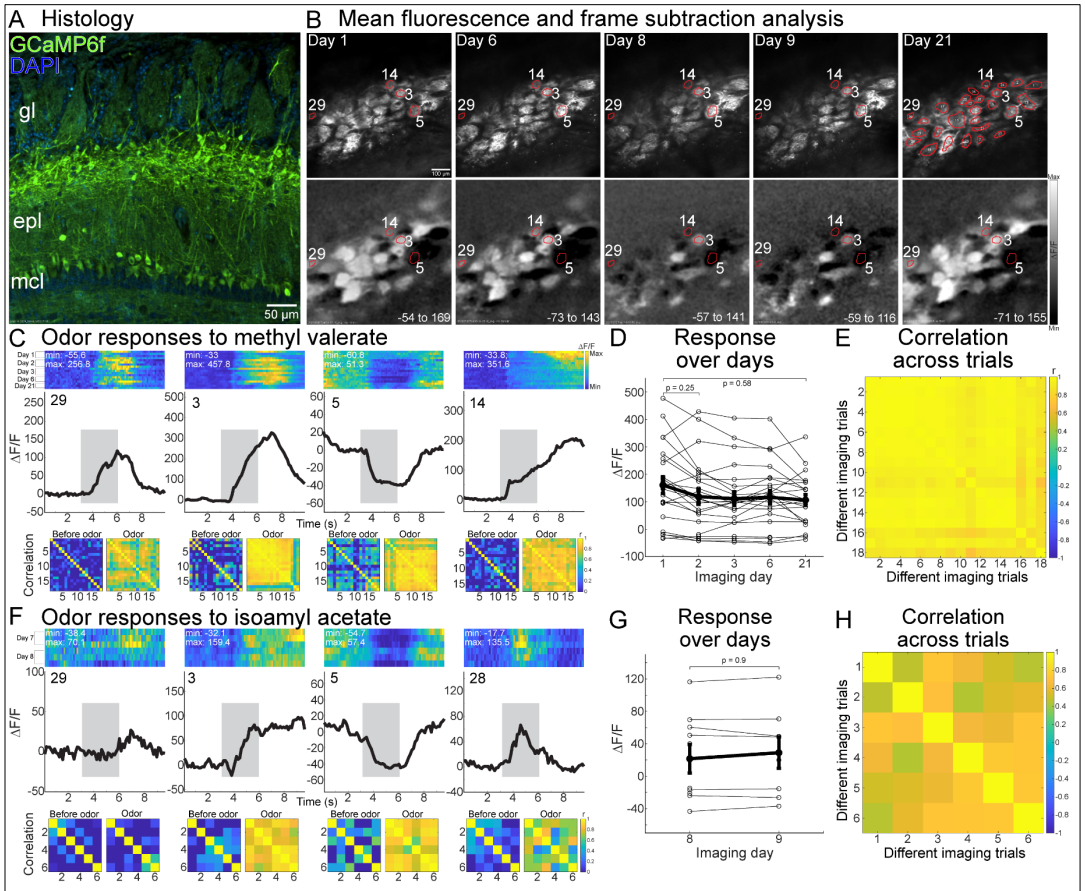

Figure 1: (**A**) Histological section illustrating endogenous GCaMP6f fluorescence from the olfactory bulb in a Tbx21::Ai148 transgenic mouse. (**B**) Mean fluorescence (*top*) and corresponding frame subtraction images (*bottom*) from 5 different imaging days in response to two different odors. The colorscales are fixed to the same range for the responses to methyl valerate and isoamyl acetate, respectively. The colorscale on the right side of the panel applies to all the frame subtraction images, and the minimum and maximum ΔF/F pixel value for each image are listed in the bottom right of each panel. (**C-E**) Response to odor methyl valerate. (**C**) (*top*) Single trial responses from multiple trials to the same odor-concentration pairing. The four regions of interest were measured in the same trials. Heat maps are scaled to the maximum response amplitude across all imaging trials for that glomerulus. The colorbar next to the rightmost panel of **C** applies to all single trial heat maps. The ΔF/F range for each glomerulus is indicated as white text in each panel. (*Middle*) Mean fluorescence time course from the single trials for each glomerulus. (*Bottom*) Correlation of individual trials for each region of interest before and during the odor stimulus. The colorbar next to the rightmost panel applies to all correlation matrices. (**D**) Mean fluorescence from all single trials across different imaging sessions. (**E**) Mean glomerular correlation across all imaging trials on the same and different days. (**F-H**) Panels follow the same arrangement as in **C-E** for responses to the odor isoamyl acetate in the same preparation. The single trial colorscale in panel **C** also applies to the single trials in panel **F**. gl, glomerular layer; epl, external plexiform layer; mcl, mitral cell layer.

147 The GCaMP6f expression facilitated the ability to image from the same glomerular population
148 across multiple experimental sessions (**Fig 1B**, each image illustrates the mean fluorescence from a
149 different imaging day in one preparation). Different odors evoked different patterns of activity across
150 the glomerular population that were similar in spatial arrangement and amplitude across different
151 imaging sessions (**Fig 1B**, bottom row, compare methyl valerate measured on days 1, 6, and 21 to
152 isoamyl acetate measured on days 8 and 9). Fluorescence time course measurements from trials
153 separated by at least 3 minutes during the same recording session, and trials carried out on different
154 imaging days had similar time course dynamics and response amplitudes (**Fig 1C**, **F**, single trial heat
155 maps are scaled to the maximum ΔF/F response from each glomerulus). Although some individual
156 glomeruli exhibited variability on different days (e.g., **Fig 1C**, ROI 14), the mean response across the
157 glomerular population was not significantly different across the different imaging sessions (**Fig 1D, G**,
158 thin lines are measurements from individual glomeruli, methyl valerate $p = 0.58$; isoamyl acetate $p =$
159 0.9, analysis only includes glomeruli in the field of view that responded to odor stimulation with at
160 least a 3 standard deviation change from baseline).
161 Odor responses from individual glomeruli measured on the same, or on different days were
162 highly correlated during (but not prior to) odor stimulation (**Fig 1C, F***,* bottom panels). The mean
163 correlation of individual glomeruli in this preparation in response to methyl valerate before and during
164 odor stimulation was 0.08 ± 0.01 and 0.62 ± 0.02, respectively (range air: -0.02 – 0.34, odor: 0.04-
165 0.95, N = 29 glomeruli). Similar results were obtained from individual glomeruli in response to isoamyl
166 acetate in this preparation (air: 0.11 ± 0.04, range -0.06-0.5; odor: 0.34 ± 0.08, range -0.02 – 0.9). The
167 correlation of the glomerular population mean was not statistically different whether the trials were
168 from the same day or from different imaging sessions (**Fig 1E**, methyl valerate: same day trials r =
169 0.95 ± 0.01 N = 24; different day trials r = 0.93 ± 0.01, N = 153; p = 0.06, **Fig 1H**, isoamyl acetate,
170 same day trials r = 0.39 ± 0.1 N = 7; different day r = 0.43 ± 0.05, N = 15; p = 0.9). Because there
171 were more samples for the same odor-concentration pairings measured on different days than on the
172 same day (e.g., typically 2-4 were taken during each imaging session), 100000 random distributions

were generated from the across day correlations of the same sample size as the within day comparisons. Relatively few of the randomly sampled across day distributions were statistically different from the same day correlations (16% and 0.02% for methyl valerate and isoamyl acetate, respectively). Therefore, the responses of individual mitral/tufted glomeruli as well as the population mean are similar in amplitude and highly correlated with themselves during odor stimulation whether the measurements are from different trials separated by a minimum of 3 minutes, or from trials taken on different days.

In each preparation-odor pairing, imaging was carried out on up to 5 different days (4 ± 0.3 imaging sessions per preparation; N = 16), separated by an average of 2.6 ± 0.5 days (range included 1-18 days between imaging sessions within the same preparation-odor pairings). To determine whether the population average changed across imaging sessions, all responsive glomeruli in each field of view were averaged together across each imaging session performed for each preparation-odor pairing. The population glomerular mean amplitude (ΔF/F) was not significantly different when imaging sessions were binned sequentially (**Fig 2A**, p = 0.77), binned relative to the absolute number of days between imaging sessions (**Fig 2B**, p = 0.83 using a Kruskal-wallis test), nor in a separate analysis restricted to preparations imaged on two consecutive days (**Fig 2B**, comparison between data

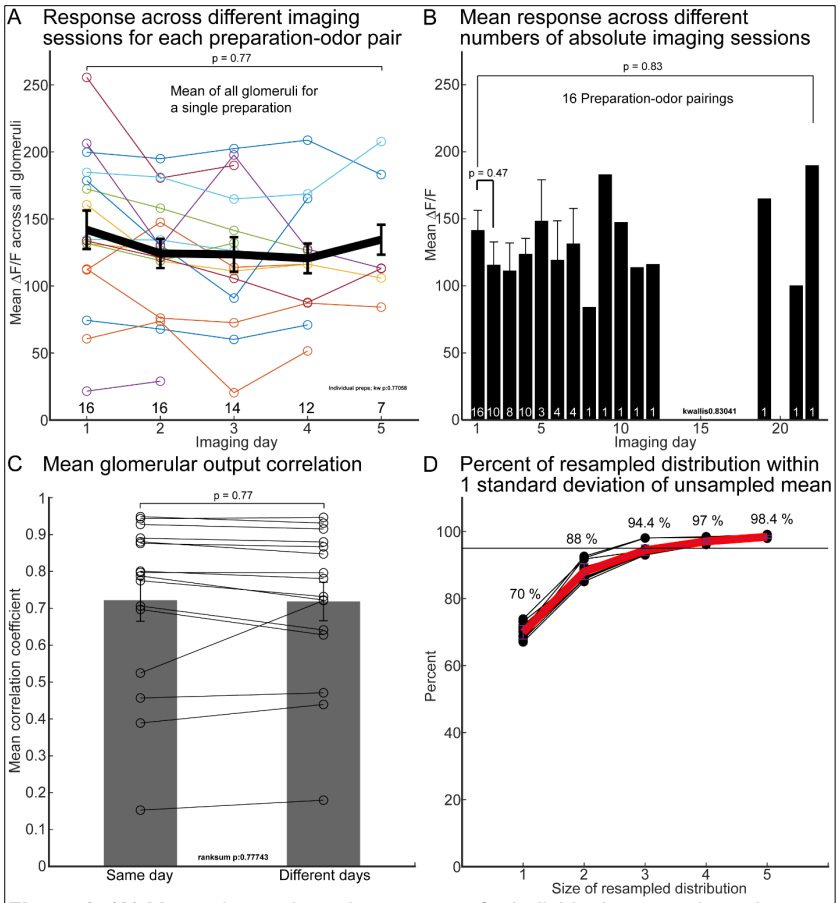

Figure 2: (**A**) Mean glomerulus-odor response for individual preparation-odor pairings (*thin lines*) and the population average (*thick line*) for different imaging sessions. The numbers at the bottom of the plot indicate the number of preparation-odor pairings on each imaging day. (**B**) The results from panel **A** binned based on the absolute number of days since the 1st imaging session. The number of preparation-odor pairing included in each mean is indicated at the bottom of each bar. (**C**) Mean correlation for different preparation-odor pairings for trials recorded on the same (*left bar*) or different days (*right bar*). (**D**) The percent of 1000 randomly sampled trials from all preparation-odor pairings that came within 1 standard deviation of the unsampled mean.

points on days 1-2, p = 0.47; 10/16 preparation-odor pairings). Consistent with these analyses, the mean correlation coefficient for trials recorded on the same day was not significantly different than those measured during different imaging sessions (**Fig 2C**, same day: 0.72 ± 0.05, different day: 0.72 ± 0.05, p = 0.77).

Although glomerular responses are stable across days, there is variability independent of adaptation effects (e.g., **Fig 1C**, *ROI29*). To identify the minimum number of trials required to obtain a representative response for a given glomerulus, we generated 1000 distributions (with replacement) of the glomerular population response by randomly selecting between 1-6 trials in response to the same preparation-odor pairing at 3.5% of saturated vapor. The data set included preparation-odor pairings in which responses were measured to 3.5% of saturated vapor in 11.43 ± 1.76 trials (range of 4-31 total trials across all imaging sessions). The 1000 distributions were averaged to create a sampled glomerular mean as a function of random samples. Randomly sampling at least 3 trials resulted in distributions with a mean that came within 1 standard deviation of the unsampled mean in 94.5% of the sampled distributions (**Fig 2D**, thin lines are from different preparation-odor pairings). This result suggests that 3 repetitions of a stimulus provide sufficient information to characterize the odor response of a single glomerulus.

Adaptation is present in subsets of MTC glomeruli in response to 6-s interstimulus intervals.

2-photon imaging was previously used to demonstrate that mitral/tufted cell glomeruli exhibit adaptation in response to odors presented with an interstimulus intervals of 6-s in anesthetized mice [22]. Because mitral/tufted cell activity and respiratory patterns can vary substantially in awake and anesthetized states, we tested whether it is present in awake mice [23, 28, 29]. The impact of repeated odor presentation is visualized in a frame subtraction analysis in which the frames during the 1st and 3rd odor presentation were subtracted (**Fig 3A-B**, Difference map, gray and black pixels indicate non-adapting and adapting glomeruli), and in which the frames during the 1st and 3rd odor presentation were subtracted from those preceding the odor stimulus (**Fig 3A-B**, 1st and 3rd odor

presentation). Both analyses illustrate that odors evoked adaptation in subsets of glomeruli within the imaging field of view (**Fig 3A-B**). This heterogeneity of adaptation is further illustrated in single trial fluorescence time course measurements from glomeruli simultaneously imaged in the same field of view (**Fig 3C-D,** regions of interest are taken from red polygons in panels **A-B**). Some glomeruli exhibit similar response amplitudes to repeated odor stimulation (**Fig 3C**, top row), while others exhibited varying degrees of decline (**Fig 3C**, middle and bottom row).

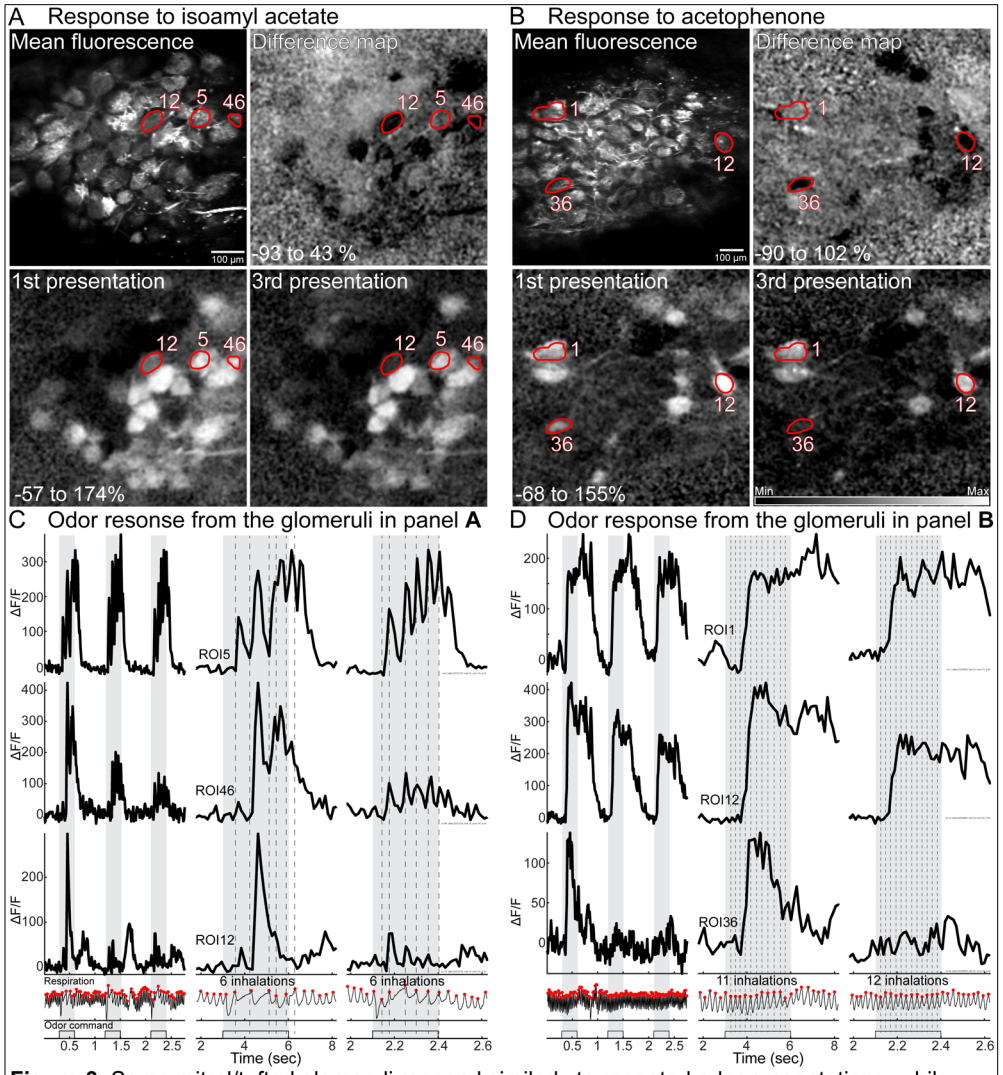

Figure 3: Some mitral/tufted glomeruli respond similarly to repeated odor presentations, while others exhibit declining responses to repeated odor presentations. (**A-B**) Mean fluorescence (*top left*) and frame subtraction analysis from two different preparation-odor pairings. The difference map (*top right*) illustrates the subtraction of the frames during the 1st and 3rd odor presentation, respectively (*bottom right panels*). The left and right preparation-odor pairings illustrate the response to isoamyl acetate and acetophenone at 3.5% and 6% of saturated vapor, respectively. The scalebar in the bottom right panel of **B** applies to all panels in **A-B**. The minimum and maximum ΔF/F frames in each frame subtraction image is indicated in the bottom left of each panel. The intensity-scaling for the frame subtraction images are both scaled to the min-max range evoked by the 1st odor presentation. (**C-D**) Single trial fluorescence time course measurements from the preparation-odor pairings in panels **A-B**. The entire recording is in the left column and the middle and right columns illustrate expanded time views of the 1st and 3rd odor presentation. The red circles in the respiration trace indicate local peaks used to determine inhalation timing. The gray bar indicates the timing of the odor command, and the vertical dashed lines indicate respiration measured during the odor presentations.

The rate and the numbers of odor inhalations can alter the amount of odor that enters the olfactory epithelium and drive adaptation in olfactory receptor neurons [8]. We tested this possibility by comparing respiratory patterns across the 1st and 3rd odor presentation within individual trials. Although respiration varied across preparations, the number of inhalations and inhalation rate within trials and across odor presentations was relatively similar (**Fig 3C-D**, dashed lines). Four additional

representative example recordings of respiration in different preparation-odor pairings illustrate that respiration activity did not consistently change throughout our odor stimulation paradigm (**Fig 4A**). The mean number of inhalations in a single exemplar preparation was not significantly different in response to the 1st and 3rd odor presentation (**Fig 4B**, 67 trials, p = 0.3; counts from the same trial are connected with a thin line). The number of inhalations during the 1st and 3rd odor presentation for all trials in this data set was not significantly different when comparing across all trials in the data set (**Fig 4C**, 1st: 10.4 ± 0.5; 3rd: 10.2 ± 0.5, p = 0.75, N = 186 trials in 8 preparations), and for comparisons of trials within individual preparations (**Fig 4D**; p-values range between 0.08-0.62 for individual preparation comparisons). Similarly, the inter-inhalation interval, which quantifies the time between two subsequent inhalations was not significantly different in the exemplar preparation (**Fig 4E**, p = 0.47) [30]. Although there was a small increase in the inter-inhalation interval between the 1st and 3rd presentation when collapsing all inhalation pairs in the data set (**Fig 4F**, P1: 284.7 ± 3.2, N = 1751; P3: 290.5 ± 2.9, N = 1723, p < 0.05), comparisons within individual preparations were not different (**Fig 4G**, p-values range between 0.09-0.84 for individual preparations). The presence of both adapting and non-adapting glomeruli measured simultaneously, and the analysis that respiratory patterns were similar in response to repeated odor presentations indicates that the mitral/tufted glomerular adaptation described here cannot be explained as variations in the odor delivery or the animals' state.

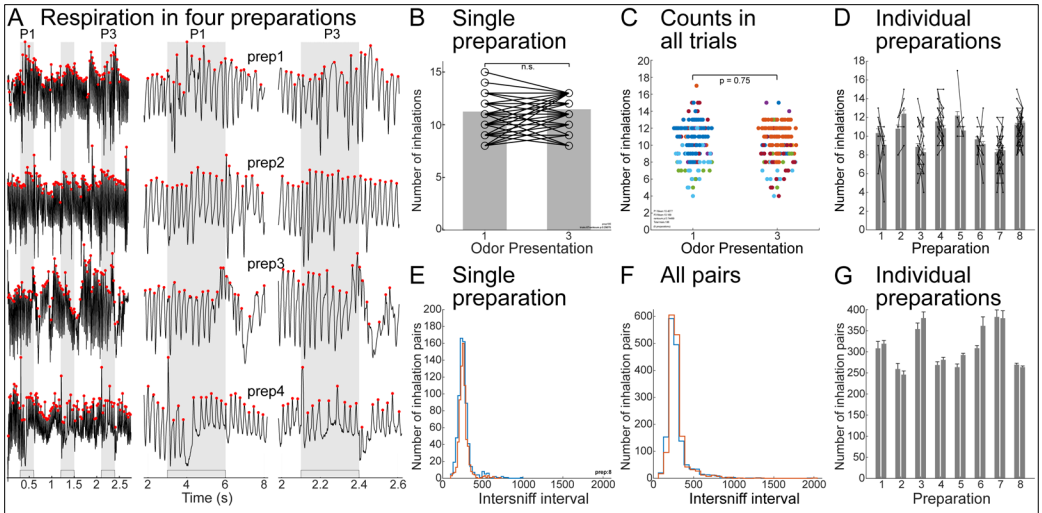

Figure 4: (**A**) Respiration measurements in four different awake mice. The left column illustrates a complete single trial; the middle and right columns illustrate expanded views during the 1st and 3rd odor presentation. The odor command signal is illustrated by the gray bars and the red circles indicate the inhalation timing values used for quantification. (**B**) Numbers of inhalations during the 1st and 3rd odor presentation from one preparation. Inhalation counts within the same trial are connected with a line. The total number of inhalations during the 1st and 3rd odor presentation was not significantly different. (**C**) Number of inhalations per trial for the population of respiratory recordings. (**D**) Mean inhalations per trial for 8 preparations. Each line indicates the number of inhalations within a trial for that preparation. (**E**) Inter-inhalation interval for the same preparation from panel **B**. (**F**) Intersniff interval for all inhalation-pairs included in panel **C**. (**G**) Mean inter-inhalation interval for inhalations during the 1st and 3rd odor presentation for 8 different preparations.

Heterogeneous adaptation across the mitral/tufted glomerular population is stable across trials.

We confirmed the reproducibility of the adaptation evoked by odors delivered with a 6-s interstimulus interval in trials imaged on the same or on different days. Glomeruli imaged simultaneously in the same field of view in four different preparation-odor pairings illustrate the presence of a non-adapting glomerulus recorded simultaneously in the same field of view as a glomerulus exhibiting adaptation to odors presented with a 6-s interstimulus interval (**Fig 5A-D**, top versus bottom row). Non-adapting glomeruli typically returned to baseline after the odor was removed. Adapting glomeruli exhibited different kinds of offset dynamics including a straightforward return to baseline (**Fig 5A**), offset responses (**Fig 5B-C**), and slow prolonged decays (**Fig 5D**). Adaptation was notable in a subset of glomeruli that exhibited a slowly decaying offset and in which subsequent odor presentations evoked suppression that increased following removal of the stimulus (**Fig 5B-C**, bottom traces). The magnitude and time course dynamics of stable and adapting glomeruli in response to the same odor-concentration pairing was remarkably stable across different trials (**Fig 5A-D**, the color scale range for the single trial heat maps are set to the minimum and maximum ΔF/F measured for each glomerulus across all trials*)*. For the non-adapting glomeruli, the response to the 1st and 3rd odor presentation was not significantly different across trials, while the four adapting glomeruli exhibited significant declines (**Fig 5**, *top versus bottom rows, inset bar graphs*).

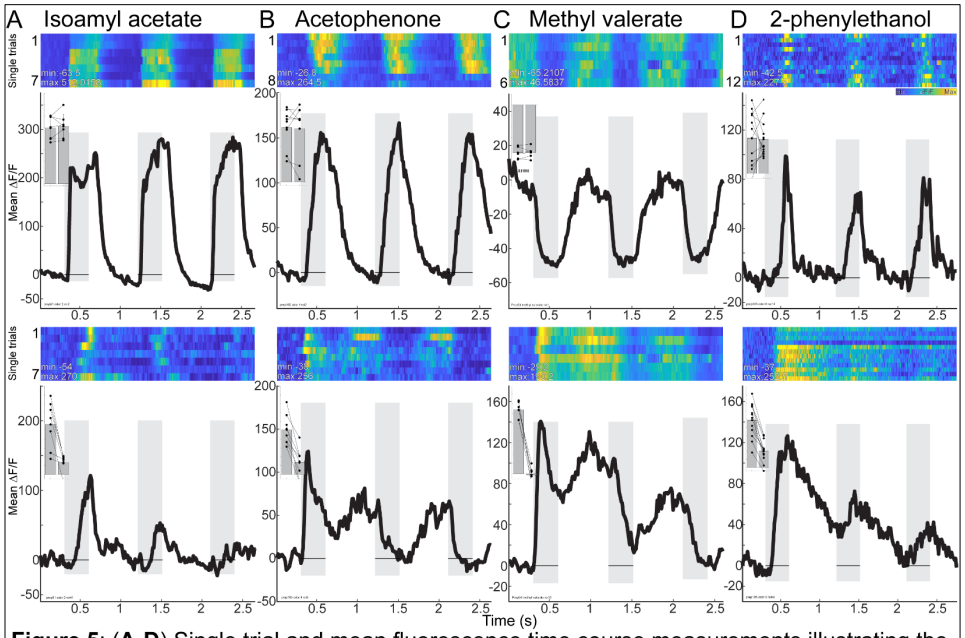

Figure 5: (**A-D**) Single trial and mean fluorescence time course measurements illustrating the presence of stable and adapting responses in the same field of view. Each column includes a pair of glomeruli simultaneously imaged from a different preparation-odor pairing. (*Top row*) Glomeruli exhibiting stable responses to repeated odor stimulation. (*Bottom row*) Glomeruli exhibiting significant adaptation. Single trial fluorescence time course from individual trials (*heat maps*) and mean (*black traces*) are illustrated for each glomerulus. The colorscale for each heatmap is fixed to the minimum and maximum response for that glomerulus and is indicated as the white text overlaid on each heat map. The response amplitude measured in each trial for the 1st and 3rd odor presentation is illustrated in the inset bar graphs with measurements from the same trial connected by a line. The comparisons for the top row are not significant ($p > 0.8$); the comparisons for the bottom row are all significant ($p < 0.005$).

Adaptation is a complicated function of concentration and interstimulus interval.

The mean fluorescence time course from four different glomeruli simultaneously imaged in the same field of view illustrates the relationship between odor concentration and interstimulus interval on adaptation (**Fig 6**). For odors delivered with an interstimulus interval of 6-s, the lowest concentration typically evoked minimal adaptation regardless of the interstimulus interval (**Fig 6A**, *blue traces*). Increasing the odor concentration resulted in non-uniform changes across the glomerular population. Repeated presentations of odor at 0.8% of saturated vapor evoked progressively weaker responses in glomerulus 1, while glomeruli 2-4 remained stable (**Fig 6A***,* green traces). Increases in odor concentration evoked progressively stronger adaptation in glomerulus 1, while glomeruli 2-3 transitioned to increasingly adapted and complex responses (**Fig 6A**, green, orange, and red traces). Glomerulus 2 responded to lower concentrations with an increase in calcium to the odor onset, which dipped below the baseline after the stimulus offset (**Fig 6A**, glomerulus 2 green trace). Higher concentrations evoked an excitatory offset response that decayed slowly, and subsequent odor presentations evoked progressively weaker responses (**Fig 6A**, glomerulus 2 orange and red trace). Glomerulus 3 responded to higher concentrations with an increase in calcium to the onset and offset of the stimulus (**Fig 6A**, glomerulus 3 orange and red traces). Subsequent odor presentations evoked a stimulus locked calcium decrease

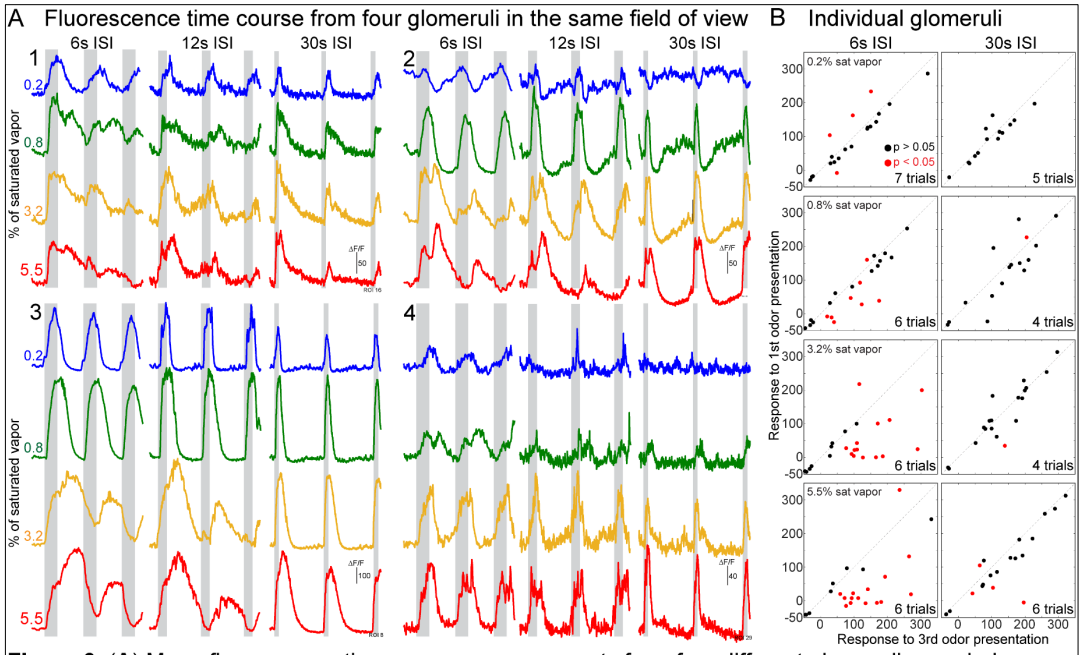

Figure 6: (**A**) Mean fluorescence time course measurements from four different glomeruli recorded simultaneously in the same field of view. Each glomerulus was measured in response to the same odor (methyl valerate) presented at different concentrations (*rows/colors*) and interstimulus intervals (*columns*). (**B**) Mean odor response amplitudes to the 1st and 3rd odor presentation across the entire glomerular population for the preparation used for the traces in panel **A**. Glomeruli are only included if they exhibited a significant response to the 1st odor presentation. Red markers indicate a glomerulus with a significantly different response to the 1st and 3rd odor presentations. The number of trials for each of the concentration and interstimulus interval conditions are indicated in the bottom right of panel **B**.

that returned to an elevated state following removal of the odor (**Fig 6A**, glomerulus 3 orange and red traces). Importantly, glomerulus 4 did not adapt at any concentrations that evoked a response (e.g., **Fig 6A**, glomerulus 4). Extending the interstimulus interval to 12-s resulted in a graded, but incomplete recovery from adaptation across the glomerular population (**Fig 6A**, 12s ISI, compare glomerulus 1-3 at 3.2% of saturated vapor). Extending the interstimulus interval to 30-s resulted in more glomeruli with non-adapting responses even at the highest concentration, although a notable few remained clearly adapted (**Fig 6A**, 30s ISI, compare glomerulus 1 and 3). The effect of concentration on adaptation on the mitral/tufted glomerular population from this preparation-odor pairing is illustrated in scatterplots of the response amplitudes evoked by the 1st and 3rd odor presentation (**Fig 6B**). More glomeruli fall beneath the diagonal line (indicating adaptation) and exhibit a significant change between the 1st and 3rd odor presentation at the higher concentrations and 6-s interstimulus interval (**Fig 6B**, red markers indicate a statistically significant change). Odors delivered with a 30-s interstimulus interval evoke responses that are closer to the diagonal and with fewer significant changes (**Fig 6B**, 30-s ISI).

Scatterplots of adaptation in individual glomeruli are illustrated for two additional preparation-odor pairings (**Fig 7A**). The number of glomeruli exhibiting significant adaptation was quantified in all preparation-odor pairings in which adaptation was measured in at least 4 single trials in response to all tested concentrations for both 6-s and 30-s interstimulus intervals (7 preparation-odor pairings; includes responses to methyl valerate, isoamyl

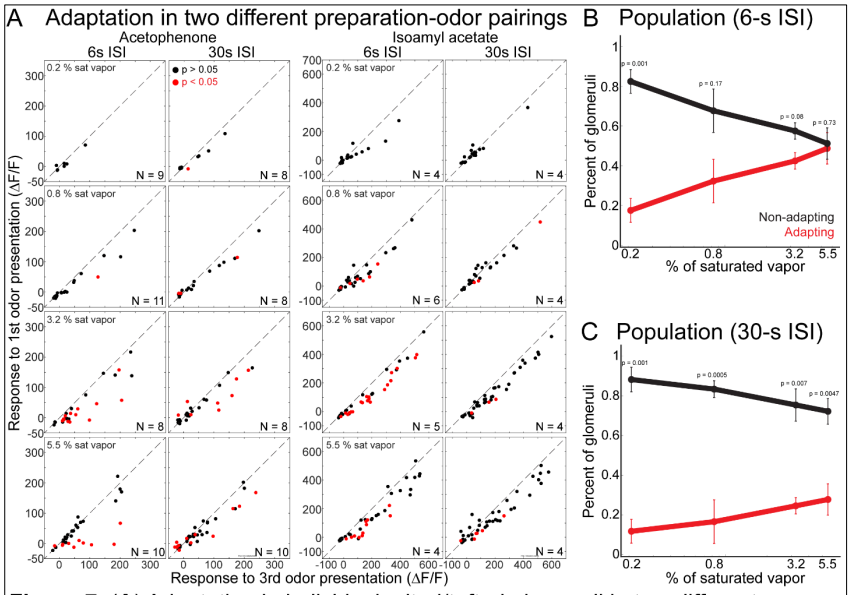

Figure 7: (**A**) Adaptation in individual mitral/tufted glomeruli in two different preparation-odor pairings at different concentrations in response to odors presented with 6-s and 30-s interstimulus intervals. Each marker indicates the mean response of a single glomerulus to the 1st and 3rd odor presentation. Red markers indicate glomeruli with significant adaptation. The number of single trials for each odor-concentration pairing are displayed in the bottom right of each panel. (**B-C**) The mean percent of responsive glomeruli in each preparation that exhibited significant adaptation (*red lines*) or responded similarly (*black lines*) in response to the 1st to the 3rd odor presentation for 6-s (**B**) and 30-s (**C**) interstimulus intervals.

acetate, benzaldehyde, acetophenone and 2-phenylethanol; 7.4 ± 1.3 trials per preparation, range of 4-17). The proportion of significantly adapting glomeruli increased with odor concentration for both 6-s and 30-s interstimulus intervals (**Fig 7B-C**). For odors delivered with a 6-s interstimulus interval, the proportion of non-adapting glomeruli was only significantly larger at the lowest tested concentration (**Fig 7B**, p-values indicated in graph). In contrast, odors delivered with a 30-s interstimulus evoked a significantly larger proportion of non-adapting glomeruli at all concentrations (**Fig 7C**, p-values indicated in graph). The number of glomeruli in the 6-s and 30-s percent calculations were not identical due to the inclusion statistical criteria, however, the mean number of glomeruli included in the 6-s and 30-s percent calculations were not significantly different from one another (0.2% 13.1 and 13.4; 0.8% 19.3 and 17.4; 3.2% 25.6 and 26.6; 5.5% 27.1 and 29.9; $p > 0.55$ for all comparisons using a ranksum test).

We quantified the response amplitude evoked by the 1st and 3rd odor presentation for all individual glomeruli and the mean glomerular response for each preparation-odor pairing (**Fig 8A-B**). The results include data from 19 preparation-odor pairings in which each odor-concentration pairing was sampled in 1-17 trials (mean number of trials for each odor-concentration pairing; 6-s interstimulus interval: 4.8 ± 0.3; 30-s interstimulus interval: 4.5 ± 0.3). At lower concentrations, individual

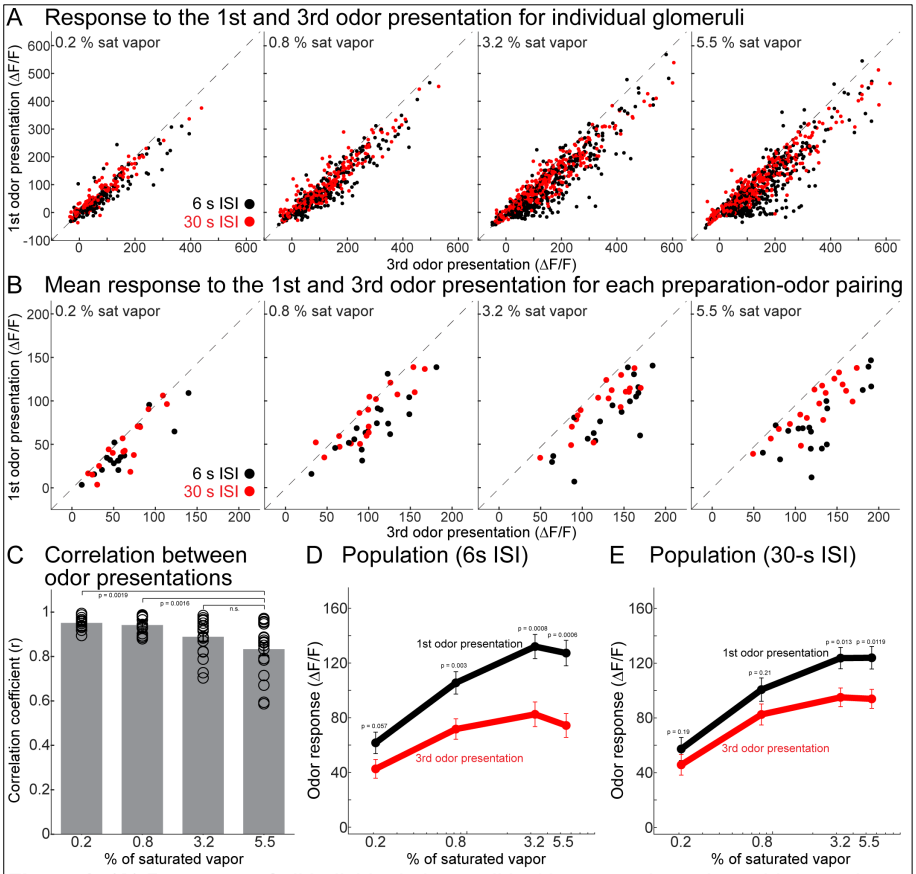

Figure 8: (**A**) Response of all individual glomeruli in 19 preparation-odor pairings to the 1st and 3rd odor presentation at 4 different concentrations. (**B**) Mean population response for each preparation- odor pairing at four different concentration pairings. Each point indicates the mean of all glomeruli that responded to the 1st odor presentation for one preparation-odor pairing. (**C**) Mean correlation of glomerular responses to the 1st and 3rd odor presentation. Each marker indicates a different preparation-odor pairing. (**D-E**) Mean response to the 1st and 3rd odor presentation as a function of odor concentration across all preparation-odor pairings for 6-s (**D**) and 30-s (**E**) interstimulus intervals.

381 glomeruli, and the mean response from each preparation fell near the diagonal at both interstimulus
382 intervals (**Fig 8A-B**, 0.2 and 0.8 % sat vapor). However, higher concentrations caused more individual
383 glomeruli, and more mean preparation-odor responses to fall below the diagonal line (**Fig 8A-B**, 3.2
384 and 5.5% sat vapor). The relationship of the response of individual glomeruli to the 1st and 3rd odor
385 presentation was highly correlated at lower concentrations and became increasingly decorrelated at
386 higher concentrations (**Fig 8C**, each marker indicates the mean correlation for one preparation-odor-
387 concentration pairing, $p < 0.01$ for comparisons of 5.5% vs 0.8% and 5.5% and 0.2 % of saturated
388 vapor*)*.

389 The impact of concentration and interstimulus interval was further quantified by measuring the
390 mean glomerular response to the 1st and 3rd odor presentation across the population of preparation-
391 odor pairing. Odors delivered with a 6-s interstimulus interval evoked significantly smaller responses
392 across the glomerular population when delivered at 0.8%, 3.2% and 5.5% of saturated vapor (**Fig 8D**,
393 the p-values are indicated in the panel; all statistics were calculated using a Wilcoxon ranksum test).
394 Separate trials in which the interstimulus interval was extended to 30-s resulted in similar odor
395 responses to the 1st odor presentation across the glomerular population at each tested concentration
396 (**Fig 8D-E**, comparison of black lines, p-value ranged between 0.35-0.96 for comparisons between
397 the 1st response during the 6-s and 30-s interstimulus interval trials). Although the response to the 3rd
398 odor presentation partly recovered with 30-s interstimulus interval, the mean response was still
399 significantly smaller at the highest tested concentrations (**Fig 8E**, p-values are indicated in the panel).
400 Therefore, adaptation is heterogeneous across the glomerular population, and higher concentrations
401 and shorter interstimulus intervals evoke higher levels of adaptation in more glomeruli.
402

403 ***Olfactory receptor neuron glomeruli exhibit minimal adaptation****.* In principle, mitral/tufted
404 adaptation could reflect changes inherited from the olfactory receptor neuron input. To test this
405 possibility, we carried out an analysis of adaptation in olfactory receptor neuron glomeruli that
406 expressed GCaMP6s using awake *in vivo* 2-photon imaging in a separate cohort of transgenic mice.

GCaMP6s was targeted to olfactory receptor neurons by mating the OMP-tTA and tetO-GCaMP6s transgenic lines. The resulting offspring that expressed both genes were confirmed in histological sections to only express GCaMP6s in the olfactory nerve layer and glomerular layer (**Fig 9A**) [31].

We restricted adaptation measurements in olfactory receptor neuron glomeruli to odors presented with a 6-s interstimulus interval at the higher concentrations that evoked the strongest adaptation in mitral/tufted glomeruli. A frame subtraction analysis for two different preparation-odor pairings illustrates that the overall activity pattern and amplitude were qualitatively similar in response to the 1st and 3rd odor presentation (**Fig 9B**). The response to the 1st and 3rd odor presentation was similarly quantified for all individual glomeruli in the data set, as well as the overall population mean for each preparation-odor pairing at three different concentrations (**Fig 9C-D**). Most glomeruli exhibited minimal adaptation, as evidenced by markers being plotted on or near the diagonal line (326 glomerulus-odor pairings in 12 preparation-odor pairings across 8 different animal preparations, includes responses to methyl valerate, isoamyl acetate and acetophenone) (**Fig**

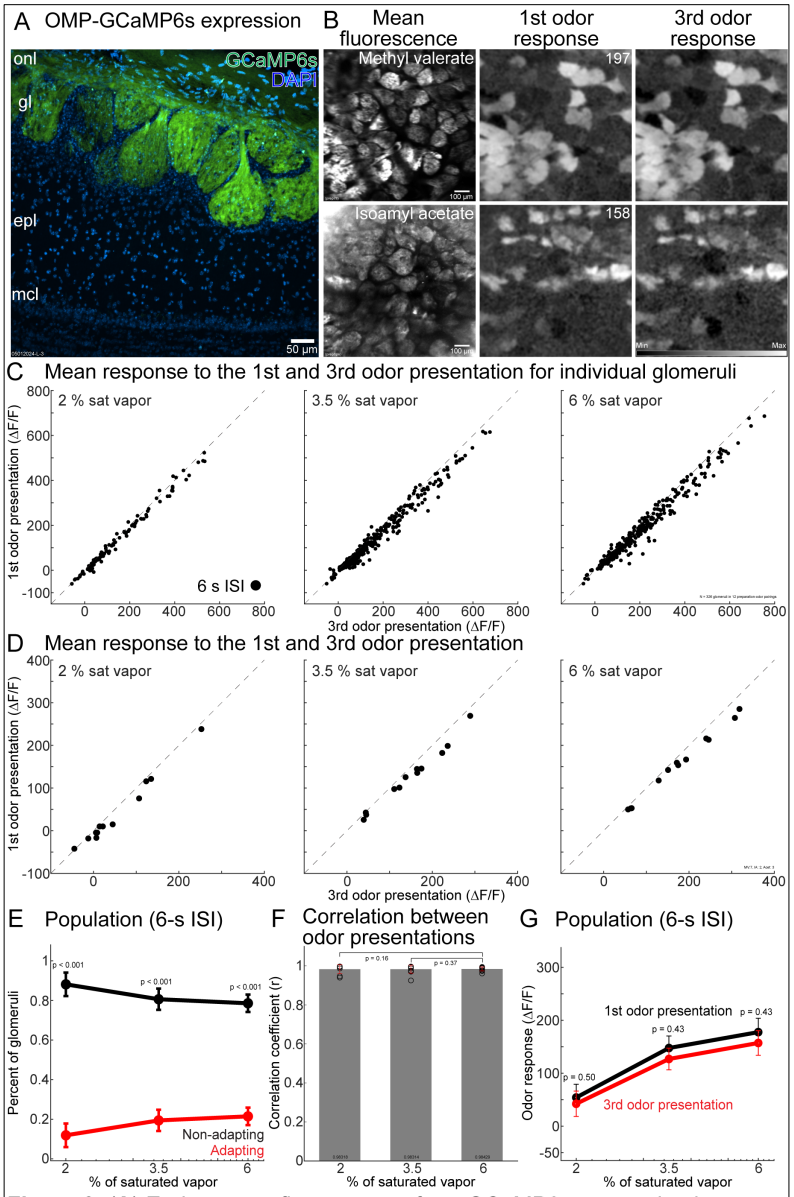

Figure 9: (**A**) Endogenous fluorescence from GCaMP6s expression in olfactory receptor neuron glomeruli. (**B**) *In vivo* fluorescence and response to two different odors. The top and bottom rows are the responses to methyl valerate and isoamyl acetate at 2 and 3.5 % of saturated vapor, respectively. The maximum ΔF/F value for each image is indicated in the top right of each panel. The color scale bar in the bottom right panel applies to all the images. (**C-D**) Response of all responsive individual glomeruli (**C**) and mean population response (**D**) for 12 preparation-odor pairings to the 1st and 3rd odor presentation at three concentration pairings. (**E**) The mean percent of responsive glomeruli in each preparation that exhibited significant adaptation (*red lines*) or responded similarly (*black lines*) to the 1st and 3rd presentation. (**F**) Mean correlation of the glomerular population for each preparation-odor pairing. (**G**) Mean response to the 1st and 3rd odor presentation as a function of odor concentration across all preparation-odor pairings. onl, olfactory nerve layer; gl, glomerular layer; epl, external plexiform layer; mcl, mitral cell layer.

433 **9C-D**). The percent of glomeruli exhibiting significant adaptation increased with odor concentration,
434 although the percent of non-adapting unchanging glomeruli was significantly higher at all
435 concentrations (**Fig 9E**). The relationship of the response of individual glomeruli to the 1st and 3rd odor
436 presentation was highly correlated (> 0.9) and did not change significantly as a function of
437 concentration (**Fig 9F**). Consistently, the mean response to the 1st and 3rd odor presentation was not
438 statistically different for the three tested odor concentrations (**Fig 9G**, p-values indicated in the panel).
439 Therefore, odors presented repeatedly with a 6-s interstimulus interval can evoke adaptation in
440 individual olfactory receptor neuron glomeruli, although the population mean is not significantly
441 impacted.
442
443
444 **Discussion**
445 We used *in vivo* 2-photon Ca^{2+} imaging in the olfactory bulb of awake mice to measure how
446 adaptation alters the responsiveness of mitral/tufted glomeruli. The same odor-concentration pairings
447 evoked stable responses across different imaging trials separated by a minimum of 3 minutes, and
448 across imaging sessions carried out on different days. However, odors presented with shorter
449 interstimulus intervals evoked adaptation heterogeneously across the glomerular population in a
450 concentration-dependent manner. Within populations of simultaneously recorded glomeruli, some
451 responded similarly, while others significantly adapted. Higher odor-concentration pairings increased
452 the proportion of significantly adapting glomeruli, more strongly decorrelated the glomerular
453 population, and attenuated the mean population response. Extending the interstimulus interval to 30-s
454 reduced the proportion of adapting glomeruli and evoked less adaptation, yet the recovery across the
455 glomerular population was incomplete. Importantly, this partial recovery is unlikely to reflect variations
456 in respiration (**Fig 4**), or adaptation inherited from the periphery (**Fig 9**). Therefore, recent odor
457 exposure can impact the transmission of olfactory sensory processing from the bulb to the rest of the
458 brain for upwards of 30 seconds. Adaptation on this timescale could be useful for mediating dynamic

459 range adjustments to complex odor environments.

460

461 ***Comparison of our results with previous studies.***

462 Our observation that mitral/tufted glomeruli exhibit relatively stable responses across different
463 imaging sessions are in contrast with another study indicating that mitral/tufted glomeruli exhibit
464 modest reductions in responsiveness over time [23]. Although these differences could reflect
465 methodological variations including a different transgenic mouse line (Pcdh21 versus Tbx21), and the
466 frequency by which the odor was delivered, our results are consistent with other studies indicating
467 that mitral/tufted glomeruli exhibit adaptation on a shorter timescale, and take upwards of 4 minutes
468 to recover from recent odor stimulation [22, 24, 25].

469 Our observations that mitral/tufted glomeruli exhibit heterogeneous adaptation reconciles past
470 work indicating that mitral cells exhibit stable responses to odor stimulation [32-35]. It seems likely
471 that the non-adapting mitral cells previously described are likely connected to the non-adapting
472 glomeruli reported here (**Fig 5A-D**, top row). The result that adaptation occurs heterogeneously is
473 also in contrast with another study that found that adaptation occurs uniformly across the mitral/tufted
474 glomerular population [24]. This difference may reflect the use of epifluorescence imaging where
475 glomerular measurements can be influenced by out-of-focus fluorescence from neighboring glomeruli.
476 In comparison, 2-photon imaging provides improved optical sectioning in the lateral and axial
477 dimensions, minimizing the impact of out-of-focus signal. Indeed, efforts to correct for diffuse
478 fluorescence in epifluorescence measurements by subtracting the background signal from each
479 glomerulus yielded less uniform adaptation [22].

480 Previous studies have reported adaptation in olfactory receptor neuron axon terminals, albeit
481 either at much higher odor concentrations than used in the present study, or in response to high
482 frequency sniffing [8, 16, 36, 37]. The mitral/tufted glomerular adaptation described here is unlikely to
483 be explained by variations in respiration since adaptation often occurred gradually over multiple
484 inhalations (**Fig 3**), and our paradigm evoked relatively similar respiratory patterns through our

recording trials (**Fig 4**). Although mice will investigate novel stimuli with bursts of high-frequency sniffing, mice typically respond to non-novel odors with respiratory rates that are consistent to what we measured (**Fig 4**) [8, 30, 38]. Furthermore, our findings of minimal adaptation in olfactory receptor neuron axon terminals and high correlation across odor repetitions are consistent with previous work from our laboratory using other calcium and voltage indicators, and the presence of minimal pattern separation across time [22, 39, 40].

A recent study imaging mitral/tufted glomeruli reported that the population representation is significantly decorrelated in response to higher sampling frequencies [41]. Our results extend those data to show that the mitral/tufted glomerular population is also transformed over time as a function of odor concentration (**Fig 8C**). Together, these studies provide evidence that processing within the bulb is involved in significantly transforming sensory input via decorrelation and other adaptive processes.

Relationship between mitral/tufted glomeruli and output signals.

Measurements from olfactory receptor neuron and mitral/tufted glomeruli reflect a kind of population average of the input from one olfactory receptor type and the apical dendrites of the mitral/tufted cells innervating a glomerulus. Although measurements from individual mitral and tufted cells are informative, identifying the neurons connected to a particular glomerulus is challenging. Consequently, interpreting single cell measurements can be challenging because differences in neural activity could reflect different sensory input [42-44]. In comparison, glomerular measurements allow for input-output comparisons in which the olfactory receptor neuron input, and the mitral/tufted output can be simultaneously measured [15, 21, 22].

Action potentials generated in mitral cell apical dendrites propagate to the soma, and somatically generated action potentials backpropagate to the apical dendrites [45]. Therefore, the apical dendrites of mitral/tufted cells innervating a glomerulus in part reflect the anatomical post-synaptic element of the input-output transformation of a glomerulus. However, subthreshold excitatory postsynaptic potentials can drive small increases in calcium that are unrelated to the presence of an

action potential, and TTX application incompletely blocks calcium signals measured from their apical dendrites in response to bath application of glutamate [23, 46]. Therefore, it seems possible that some proportion of calcium measurement from mitral/tufted glomeruli could reflect subthreshold activity. Future experiments would benefit from development of genetically encoded voltage indicators that are specifically tuned to supra-threshold voltage changes to allow for unambiguous optical measurements of spiking activity from mitral/tufted apical dendrites innervating a glomerulus [47]. Alternatively, improvements in methods to selectively target the neurons associated with a parent glomerulus would provide the ability to perform calcium and voltage imaging from mitral/tufted cell bodies to help resolve this issue [42, 44].

Mechanisms underlying adaptation and functional relevance.

The presence of glomeruli that exhibit gradually decreasing responses, while others exhibited elevated activity levels suggest that multiple mechanisms may be involved in mitral/tufted glomerular adaptation (e.g., **Fig 6**, ROIs 1 versus 3). Recurrent inhibition can shape the spiking activity of mitral cells in a manner that depends on the overall activation of the mitral cell itself [32]. The mechanism is likely to be complex since granule cells exhibit strong paired pulse depression, suggesting that strongly activated granule cells should provide progressively weaker inhibition onto their synaptic contacts [48]. The specific combination of receptors expressed on different cell types is also likely to be important since NMDA antagonism can impair habituation to odor stimuli *in vivo* [49]. Feedback from other brain areas is another candidate mechanism since stimulating acetylcholine input to the bulb dishabituates glomerular and behavioral sensitivity [25]. The presence of a concentration-dependent form of adaptation is compatible with a model of lateral inhibition whereby higher concentrations of an odor must drive input to increasing numbers of glomeruli by activating lower affinity olfactory receptors. This process should increase the magnitude of lateral inhibition in the bulb [15, 16, 21, 50]. Such a mechanism could account for the heterogeneity of different adapting responses since each glomerulus is likely to be differently influenced by lateral circuits [51]. This

537 hypothesis can be tested in future studies by modulating the magnitude of lateral inhibition within the
538 circuit by selectively manipulating specific olfactory receptor neuron or interneuron types within the
539 bulb [50, 52].
540
541 ***Estimating variability within the mitral/tufted glomerular population.***
542 Neural measurements in awake mice are more variable than in anesthetized preparations in
543 part due to the variable nature of respiration in awake mice. Although it is possible to control the
544 frequency of respiration in anesthetized preparations, such methods would be challenging to
545 implement in awake preparations [41, 53]. Here we purposely oversampled the number of trials for
546 each odor-concentration pairing and found that despite minor variations in respiration (**Figs 3-4**), the
547 general response time course dynamics and amplitudes were surprisingly similar (**Fig 5**). Our
548 sampling analysis found that a minimum of 3 samples are needed to recapitulate a reasonable
549 estimate of the response from a glomerulus measured in a larger number of samples. These data
550 demonstrate that mitral/tufted glomerular signals are surprisingly consistent despite respiratory
551 variations and provide a starting point for establishing sample sizes for future experiments.
552
553 ***Conclusions.***
554 Here we extend previous work describing a form of adaptation in mitral/tufted glomeruli that
555 occurs on timescales that could be relevant for the process of odor-background segmentation. Future
556 studies are needed to confirm the functional and behavioral relevance of these processes.
557 Simultaneous comparisons of olfactory receptor neuron input and mitral/tufted glomerular output will
558 provide insight into the nature of how the olfactory bulb can transform a stable sensory input into an
559 adapting output. Comparisons of mitral/tufted glomeruli before and after adaptation has taken place
560 will define whether these adaptive processes alter processing by compressing or shifting the dynamic
561 range of individual neurons [7, 10, 54]. Finally, although there is evidence that mice behaviorally
562 habituate to odors presented on similar timescales, simultaneous imaging from mitral/tufted glomeruli

563 during a behavioral assay is necessary to clearly link glomerular measurements with perception.

564

565

566 **Methods**

567 ***Transgenic mice.***

568 GCaMP6f was targeted to mitral/tufted glomeruli by mating the Ai148 GCaMP6f transgenic
569 reporter line (Jax stock #030328) to the Tbx21-cre transgenic line (Jax stock #024507). GCaMP6s
570 was targeted to olfactory receptor neuron glomeruli by mating the tetO-GCaMP6s transgenic reporter
571 line (Jax stock #024742) to the OMP-tTA transgenic line (Jac stock #017754) [31]. Offspring that
572 expressed eGFP and Cre recombinase (mitral/tufted glomeruli), or eGFP and tTA (olfactory receptor
573 neurons glomeruli) were used for experiments. Genotyping was performed by Transnetyx (Cordova,
574 TN). Appropriate targeting of either GCaMP to olfactory receptor neurons or mitral/tufted glomeruli
575 was also confirmed histologically in a subset of the preparations based on endogenous fluorescence
576 expression.

577

578 ***Surgical procedures.***

579 All procedures were approved by the Florida State University Animal Care and Use
580 Committee. Male and female adult (> 21 days) transgenic mice were anesthetized using
581 ketamine/xylazine (90 / 10 mg/kg, Zoetis, Kalamazoo, MI), placed on a heating pad and had
582 ophthalmic ointment applied to their eyes. Mice were given a pre-operative dose of carprofen (10
583 mg/kg, Zoetis, Kalamazoo, MI), atropine (0.2 mg/kg, Covetrus, Dublin, OH), dexamethasone (4
584 mg/kg, Bimeda, La Sueur, MN), and bupivacaine (2.5 mg/kg, Hospira, Lake Forest, IL). Fur was
585 removed from the top of the skull using a depilatory agent, and the skin was scrubbed with 70%
586 isopropyl alcohol and iodine (Covidien, Mansfield, MA). An incision was made to remove the skin over
587 the skull and blunt dissection was used to remove the underlying membrane. Dental cement
588 (Metabond, Covetrus, Dublin, OH) was used to attach a custom headpost to the skull, which was held

589 using a custom headpost holder. After the cement finished drying, the bone above the olfactory bulb
590 was either thinned using a dental drill (Osada, XL-230, Los Angeles, CA) and covered with
591 cyanoacrylate to improve optical clarity or was removed and replaced with #1 cover glass. Upon
592 completion of the surgery, the mouse was allowed to recover on a heating pad until they were fully
593 ambulatory. Animals were given a post-operative analgesic at the end of the day of surgery and for at
594 least 3 days post-operatively.
595
596 ***Histology***.
597 Mice were euthanized (euthasol) following imaging and either underwent cardiac perfusion
598 with phosphate buffered saline and 4% paraformaldehyde or had their brains directly extracted and
599 post-fixed in 4% paraformaldehyde before being cut on a vibratome in 40 μm sections (Leica
600 VT1000S, Deer Park, IL). Sections through the olfactory bulb were mounted on slides and were
601 coverslipped using Fluoromount-G containing DAPI (SouthernBiotech, Birmingham, AL). Endogenous
602 fluorescence expression of GCaMP6f or GCaMP6s was observed using a GFP filter set on either a
603 Zeiss Axioskop epifluorescence microscope or a Nikon CSU-W1 spinning disk confocal microscope.
604
605 ***2-photon imaging***.
606 Imaging was performed using a Sutter MOM 2-photon microscope equipped with an 8 kHz
607 (30.9 Hz) resonant scanner (Cambridge Technology, USA) and an emission pathway equipped with a
608 GaAsP PMT (#H10770PA-40-04, Hamamatsu, Japan). Laser excitation was provided using a
609 Spectra-Physics DS+ between 940-980 nm with power modulated by a Pockels cell (Model #350-
610 105-02, Conoptics, Danbury, CT), or an Alcor 920 at 920 nm with power modulated by an internal
611 acousto-optic modulator. Imaging was performed using a Nikon 16x 0.8 N.A. or a custom 10x 0.5
612 N.A. objective lens. Laser power was confirmed to be less than 150 mW at the output of the objective
613 lens measured using a power meter (Newport 843-R) for scanning areas ranging between 711 μm^2
614 (16 x lens) and 1138 μm^2 (10x lens).

615

616 ***Odorant delivery***.

617 Odorants included: methyl valerate, isoamyl acetate, benzaldehyde, ethyl butyrate,
618 acetophenone (A12727 Lot #10204758), and 2-phenylethanol (77861-250ML, LOT # STBJ1505)
619 (Sigma-Aldrich, USA) were used at concentrations between 0.05 and 6 % of saturated vapor. For
620 mitral/tufted glomerular measurements, the olfactometer design involved air being pushed through
621 vials of pure odor using a syringe pump (NE-1000, PumpSystems, Farmingdale, NY) running at
622 different flow rates (0.25 – 28 ml /min). This odor stream underwent an initial air dilution with a lower
623 flow rate of clean air (30 ml/min). The resulting odorized air stream connected to a dual 3-way
624 solenoid valve (360T041, NResearch, West Caldwell, NJ), which was connected to an exhaust, a
625 clean air stream, and a delivery manifold which served as the final delivery apparatus. The delivery
626 valve was connected to a Teflon delivery manifold placed in front of the mouse's nose, which had a
627 higher flow rate of clean air constantly flowing through it (450 ml/min). Prior to odor triggering, the
628 solenoid sent the odorized air stream to the exhaust, and the clean air into the delivery manifold,
629 while triggering it caused the odor to be injected into the delivery manifold where it underwent a
630 second air dilution. For olfactory receptor neuron glomerular measurements, the olfactometer design
631 was similar except air flow was controlled by mass flow controllers (Alicat, MC-100SCCM and MC-
632 1SLPM), and underwent only a single air dilution step [55]. The odor delivery time-course for both
633 odor delivery systems were confirmed using a photoionization detector (200C, Aurora Scientific,
634 Aurora, ON).

635

636 ***Imaging procedures***.

637 Prior to data collection mice were positioned underneath the microscope and the angle of the
638 headpost holder was adjusted to optimize the imaging field of view. The headpost holder position was
639 then locked into place so that the mouse could be precisely realigned during future imaging sessions.
640 During data collection, awake head-fixed mice were placed underneath the microscope objective with

641 the olfactometer and a thermocouple (to measure respiration, Omega 5TC-TT-K-36-36, Newark) near
642 its nose. The signals from the respiration sensor were amplified and low-pass filtered using a
643 differential amplifier (Model 3000, AM-Systems, Sequim, WA), which was simultaneously recorded by
644 the imaging system at 1000 Hz. Odor-stimulation trials took place in the form of different odor-
645 concentration pairings delivered in three consecutive presentations with interstimulus intervals of 6,
646 12 and 30 seconds. Individual trials were separated by a minimum of 3 minutes. Odor-concentration
647 pairings included 4 steps between 0.2 – 5.5% of saturated vapor. Measuring the response to the full
648 range of concentrations for a particular odor was prioritized within a single imaging session for at
649 least one interstimulus interval. The response to the same odor-concentration-interstimulus interval
650 pairing was typically measured in at least two consecutive trials to assess within-day, across-trial
651 repeatability. If time permitted, the response to the same odor-concentration pairings were measured
652 to a different interstimulus interval. Mitral/tufted glomerular imaging took place on up to 5 different
653 sessions up to 35 days apart.
654
655 ***Data analysis***
656 ***Processing and segmentation****.*
657 Following data acquisition, the raw image files were spatially and temporally averaged from
658 512x512 pixels sampled at 30.9 Hz to 256x256 pixels sampled at 7.72 Hz. The resulting data were
659 exported to TIFF format for all subsequent analysis. Because the mice were typically calm, motion
660 correction was not used. However, occasional recordings with sufficient motion artifact that made it
661 impossible to interpret the measurements were discarded from the subsequent analysis pipeline.
662 Segmentation of image stacks into glomerular regions of interest was manually carried out in custom
663 software (Turbo-SM, SciMeasure, Decatur, GA). Glomeruli were identified as glomerular sized
664 regions of interest using the mean fluorescence within a trial, as well as a frame subtraction analysis
665 that displays the difference between the frames during and prior to the odor stimulation. The pixel
666 areas containing the regions of interest were saved and the fluorescence time course values from

667 each region of interest were extracted for subsequent analysis. All fluorescence time course traces
668 were converted to ΔF/F by dividing each trace by the mean of all the frames prior to odor stimulation
669 (typically 23).
670
671 ***Image analysis.***
672 The mean fluorescence and frame subtraction images are from the average of at least two
673 single trials (e.g., **Fig 1B**, **Fig 3A-B, Fig 9B**). The mean fluorescence images are generated from the
674 average of all the frames during the imaging trial. The frame subtraction images were generated by
675 subtracting 19 frames during odor stimulation from 9 frames prior to the stimulus (**Fig 1B**, *bottom row*;
676 **Fig 3A-B**, *1st and 3rd presentation*). The frame subtraction difference images were generated by
677 subtracting 20 frames during the 3rd odor presentation from 20 frames during the 1st presentation (**Fig**
678 **3A-B**, *difference map*). The frame subtraction images underwent at least two passes of a low-pass
679 spatial filter and were converted to ΔF/F by dividing the fluorescence value of each pixel by the mean
680 of at least 60 consecutive frames in the image stack in Turbo-SM.
681
682 ***Calculating response amplitude.***
683 Odor responses (ΔF/F) were calculated as the largest difference between a 1200 msec
684 temporal window during the peak of the odor response and the time prior to odor stimulation. This
685 value was calculated independently for each glomerulus.
686
687 ***Correlation analysis methods.***
688 Across trial correlations were calculated by measuring the correlation between the 2.5 seconds
689 prior to odor stimulation, and during odor stimulation for individual traces (**Fig 1C**, **F**), and for the
690 mean population response across all glomeruli in a field of view (**Fig 1E**, **H**). The mean glomerular
691 output correlation analysis (**Fig 2C**) was generated by averaging the correlation coefficients from all
692 trials on the same day or all trial pairings that took place on different days (**Fig 1E, H**).

693

694 ***Amplitude across time methods.***

695 The mean amplitude across imaging sessions was calculated by averaging the odor-evoked
696 response (ΔF/F) of all responsive glomeruli from each imaging session (**Fig 1D, G**). Non-responsive
697 glomeruli were excluded from this analysis to prevent them from biasing the analysis in the direction
698 of not changing. Glomeruli were identified as responsive if odor stimulation evoked a minimum of a 3
699 standard deviation change from the pre-odor period (thresholds ranged between 3-6, 4.6 ± 0.3, N =
700 16 preparation-odor pairings). Testing for statistical differences during different imaging sessions was
701 performed using the Wilcoxon rank sum test (ranksum function in MATLAB), and the Kruskal-wallis
702 test (kruskalwallis function in MATLAB). Because the number of imaging sessions, and the time
703 between each imaging session was not the same for each preparation, population responses are
704 illustrated binned across different imaging sessions or based on the number of days since the 1st
705 imaging session (**Fig 2A-B**, the number of preparation-odor pairings included in each bin are
706 indicated at the bottom of each graph).

707

708 ***Datasampling methods.***

709 The random sampling analysis was calculated by generating 1000 random distributions (with
710 replacement) of the glomerular mean (**Fig 2D**, datasample function in MATLAB). All trials for each
711 preparation were tested in response to the same odor-concentration pairing (typically 3.2 % of
712 saturated vapor). Larger number of random distributions yielded similar results.

713

714 ***Respiration analysis.***

715 Individual inhalations were identified in the respiration traces using the islocalmax function in
716 MATLAB. Inhalation counts were measured by counting the number of inspirations while the odor
717 command was on. Inter-inhalation intervals were calculated by measuring the time between
718 subsequent inhalations using the diff function in MATLAB.

719

720 ***Adaptation analysis***.

721 To avoid biasing the analysis in the direction of non-adapting, glomeruli were only included in
722 the analysis if they responded to the 1st odor presentation with at least a 3 standard deviation change
723 from the baseline fluorescence. Consequently, the number of glomeruli is not identical for the 6-s and
724 30-s analyses due to differences in numbers of trials and signal-to-noise ratio for different
725 preparation-odor pairings. For single mitral/tufted glomeruli comparisons, statistical significance was
726 assessed using a non-parametric Wilcoxon rank sum test for measurements in response to the 1st or
727 3rd odor presentation (**Fig 6B, Fig 7A**). Mitral/tufted glomeruli preparation-odor pairings were only
728 included in the mean percent analysis if all odor-concentration pairings were sampled in a minimum
729 of 4 trials (**Fig 7B-C**). The number of significantly adapting glomeruli was calculated by comparing the
730 responses to the 1st and 3rd odor presentation using a Wilcoxon ranksum test (e.g., the bar graphs in
731 **Fig 5**). The correlation between the 1st and 3rd odor presentation was performed by calculating the
732 correlation of all significantly responsive glomeruli at each odor concentration (**Fig 8C, 9F**). For the
733 population analysis of the impact of concentration and interstimulus interval on adaptation (**Fig 8D-E,**
734 **9G**), the mean glomerular response to the 1st and 3rd odor presentation was calculated for each
735 preparation-odor pairing using all glomeruli that responded to the 1st presentation with at least a 3
736 standard deviation change. A Wilcoxon ranksum test was used to test for significant differences for
737 each of the different concentrations.

738

739 **Acknowledgements**

740 This work was supported by funding from NIDCD R01 DC020519, and internal funds from
741 Florida State University. We are grateful to Dr. Evan Lloyd for critical comments on an early draft of
742 this manuscript.

743 **Data Sharing and Data Availability:** Data will be made available upon request from the corresponding
744 author.

745

746

747

748

749

750 **Figure Legends**

751 **Fig 1**: (**A**) Histological section illustrating endogenous GCaMP6f fluorescence from the olfactory bulb
752 in a Tbx21::Ai148 transgenic mouse. (**B**) Mean fluorescence (top) and corresponding frame
753 subtraction images (bottom) from 5 different imaging days in response to two different odors. The
754 frame subtraction color scales are fixed to the same range for the responses to methyl valerate and
755 isoamyl acetate, respectively. The color scale on the right side of the panel applies to all the frame
756 subtraction images, and the minimum and maximum $\Delta F/F$ pixel value for each image are listed in the
757 bottom right of each panel. (**C**-**E**) Response to odor methyl valerate. (**C**) (top) Single trial responses
758 from multiple trials to the same odor-concentration pairing. The four regions of interest were
759 measured in the same trials. Heat maps are scaled to the maximum response amplitude across all
760 imaging trials for that glomerulus. The colorbar next to the rightmost panel of **C** applies to all single
761 trial heat maps. The $\Delta F/F$ range for each glomerulus is indicated as white text in each panel. (Middle)
762 Mean fluorescence time course from the single trials for each glomerulus. (Bottom) Correlation of
763 individual trials for each region of interest before and during the odor stimulus. The colorbar next to
764 the rightmost panel applies to all correlation matrices. (**D**) Mean fluorescence from all single trials
765 across different imaging sessions. (**E**) Mean glomerular correlation across all imaging trials on the
766 same and different days. (**F**-**H**) Panels follow the same arrangement as in **C**-**E** for responses to the
767 odor isoamyl acetate in the same preparation. The single trial color scale in panel **C** also applies to
768 the single trials in panel F. gl, glomerular layer; epl, external plexiform layer; mcl, mitral cell layer.

769

770 **Fig 2**: (**A**) Mean glomerulus-odor response for individual preparation-odor pairings (thin lines) and the
771 population average (thick line) for different imaging sessions. The numbers at the bottom of the plot
772 indicate the number of preparation-odor pairings on each imaging day. (**B**) The results from panel A
773 binned based on the absolute number of days since the 1st imaging session. The number of
774 preparation-odor pairings included in each mean is indicated at the bottom of each bar. (**C**) Mean
775 correlation for different preparation-odor pairings for trials recorded on the same (left bar) or different
776 days (right bar). (**D**) The percent of 1000 randomly sampled trials from all preparation-odor pairings
777 that came within 1 standard deviation of the unsampled mean.
778
779 **Fig 3**: Some mitral/tufted glomeruli respond similarly to repeated odor presentations, while others
780 exhibit adaptation to repeated odor presentations. (**A**-**B**) Mean fluorescence (top left) and frame
781 subtraction analysis from two different preparation-odor pairings. The difference map (top right)
782 illustrates the subtraction of the frames during the 1st and 3rd odor presentation, respectively (bottom
783 right panels). The left and right preparation-odor pairings illustrate the response to isoamyl acetate
784 and acetophenone at 3.5% and 6% of saturated vapor, respectively. The scalebar in the bottom right
785 panel of **B** applies to all panels in **A**-**B**. The minimum and maximum $\Delta F/F$ frames in each frame
786 subtraction image is indicated in the bottom left of each panel. The intensity-scaling for the frame
787 subtraction images are both scaled to the min-max range evoked by the 1st odor presentation. (**C**-**D**)
788 Single trial fluorescence time course measurements from the preparation-odor pairings in panels **A**-**B**.
789 The entire recording is in the left column and the middle and right columns illustrate expanded time
790 views of the 1st and 3rd odor presentation. The red circles in the respiration trace indicate local peaks
791 used to determine inhalation timing. The gray bar indicates the timing of the odor command, and the
792 vertical dashed lines indicate respiration signals measured during the odor presentations.
793
794 **Fig 4**: (**A**) Respiration measurements in four different awake mice. The left column illustrates a
795 complete single trial; the middle and right columns illustrate expanded views during the 1st and 3rd

odor presentation. The odor command signal is illustrated by the gray bars and the red circles indicate the inhalation timing values used for quantification. (**B**) Numbers of inhalations during the 1st and 3rd odor presentation from one preparation. Inhalation counts within the same trial are connected with a line. The total number of inhalations during the 1st and 3rd odor presentation was not significantly different. (**C**) Number of inhalations per trial for the population of respiratory recordings. (**D**) Mean inhalations per trial for 8 preparations. Each line indicates the number of inhalations within a trial for that preparation. (**E**) Inter-inhalation interval for the same preparation from panel **B**. (**F**) Inter-inhalation interval for all inhalation-pairs included in panel **C**. (**G**) Mean inter-inhalation interval for inhalations during the 1st and 3rd odor presentation for 8 different preparations.

Fig 5: (**A-D**) Single trial and mean fluorescence time course measurements illustrating the presence of stable and adapting responses in the same field of view. Each column includes a pair of glomeruli simultaneously imaged from a different preparation-odor pairing. (Top row) Glomeruli exhibiting stable responses to repeated odor stimulation. (Bottom row) Glomeruli exhibiting significant adaptation. Single trial fluorescence time course from individual trials (heat maps) and mean (black traces) are illustrated for each glomerulus. The color scale for each heatmap is fixed to the minimum and maximum response for that glomerulus and is indicated as the white text overlaid on each heat map. The response amplitude measured in each trial for the 1st and 3rd odor presentation is illustrated in the inset bar graphs with measurements from the same trial connected by a line. The comparisons for the top row are not significant ($p > 0.8$); the comparisons for the bottom row are all significant ($p < 0.005$).

Fig 6: (**A**) Mean fluorescence time course measurements from four different glomeruli recorded simultaneously in the same field of view. Each glomerulus was measured in response to the same odor (methyl valerate) presented at different concentrations (rows/colors) and interstimulus intervals (columns). (**B**) Mean odor response amplitudes to the 1st and 3rd odor presentation across the entire

822 glomerular population for the preparation used for the traces in panel **A**. Glomeruli are only included if
823 they exhibited a significant response to the 1st odor presentation. Red markers indicate a glomerulus
824 with a significantly different response to the 1st and 3rd odor presentations. The number of trials for
825 each of the concentration and interstimulus interval conditions are indicated in the bottom right of
826 panel **B**.
827
828 **Fig 7**: (**A**) Adaptation in individual mitral/tufted glomeruli in two different preparation-odor pairings at
829 different concentrations in response to odors presented with 6-s and 30-s interstimulus intervals.
830 Each marker indicates the mean response of a single glomerulus to the 1st and 3rd odor
831 presentation. Red markers indicate glomeruli with significant adaptation. The number of single trials
832 for each odor-concentration pairing are displayed in the bottom right of each panel. (**B**-**C**) The mean
833 percent of responsive glomeruli in each preparation that exhibited significant adaptation (red lines) or
834 responded similarly (black lines) in response to the 1st to the 3rd odor presentation for 6-s (**B**) and
835 30-s (**C**) interstimulus intervals.
836
837 **Fig 8**: (**A**) Response of all individual glomeruli in 19 preparation-odor pairings to the 1st and 3rd odor
838 presentation at 4 different concentrations. (**B**) Mean population response for each preparation- odor
839 pairing at four different concentration pairings. Each point indicates the mean of all glomeruli that
840 responded to the 1st odor presentation for one preparation-odor pairing. (**C**) Mean correlation of
841 glomerular responses to the 1st and 3rd odor presentation. Each marker indicates a different
842 preparation-odor pairing. (**D**-**E**) Mean response to the 1st and 3rd odor presentation as a function of
843 odor concentration across all preparation-odor pairings for 6-s (**D**) and 30-s (**E**) interstimulus intervals.
844
845 **Fig 9**: (**A**) Histological section from the olfactory bulb illustrating the endogenous fluorescence from
846 GCaMP6s expression in olfactory receptor neuron glomeruli. (**B**) *In vivo* fluorescence and response
847 to two different odors. The top and bottom rows are the responses to methyl valerate and isoamyl

848 acetate at 2 and 3.5 % of saturated vapor, respectively. The maximum ΔF/F value for each image is
849 indicated in the top right of each panel. The color scale bar in the bottom right panel applies to all the
850 images. (**C**-**D**) Response of all responsive individual glomeruli (**C**) and mean population response (**D**)
851 for 12 preparation-odor pairings to the 1st and 3rd odor presentation at three concentration pairings.
852 (**E**) The mean percent of responsive glomeruli in each preparation that exhibited significant
853 adaptation (red lines) or responded similarly (black lines) to the 1st and 3rd presentation. (**F)** Mean
854 correlation of the glomerular population for each preparation-odor pairing. (**G**) Mean response to the
855 1st and 3rd odor presentation as a function of odor concentration across all preparation-odor pairings.
856 onl, olfactory nerve layer; gl, glomerular layer; epl, external plexiform layer; mcl, mitral cell layer.
857
858
859
860
861
862
863
864
865
866
867
868
869
870
871
872
873

References

1. Homma R, Cohen LB, Kosmidis EK, Youngentob SL. Perceptual stability during dramatic changes in olfactory bulb activation maps and dramatic declines in activation amplitudes. Eur J Neurosci. 2009;29(5):1027-34. doi: 10.1111/j.1460-9568.2009.06644.x. PubMed PMID: 19291227; PubMed Central PMCID: PMC2762425.
2. Gross-Isseroff R, Lancet D. Concentration-dependent changes of perceived odor quality. Chemical Senses. 1988;13(2):191-204. doi: 10.1093/chemse/13.2.191.
3. Uchida N, Mainen ZF. Odor concentration invariance by chemical ratio coding. Front Syst Neurosci. 2007;1:3. doi: 10.3389/neuro.06.003.2007. PubMed PMID: 18958244; PubMed Central PMCID: PMC2526272.
4. Weber AI, Fairhall AL. The role of adaptation in neural coding. Curr Opin Neurobiol. 2019;58:135-40. doi: 10.1016/j.conb.2019.09.013. PubMed PMID: 31569061.
5. Wark B, Lundstrom BN, Fairhall A. Sensory adaptation. Curr Opin Neurobiol. 2007;17(4):423-9. doi: 10.1016/j.conb.2007.07.001. PubMed PMID: 17714934; PubMed Central PMCID: PMC2084204.
6. Whitmire CJ, Stanley GB. Rapid Sensory Adaptation Redux: A Circuit Perspective. Neuron. 2016;92(2):298-315. doi: 10.1016/j.neuron.2016.09.046. PubMed PMID: 27764664; PubMed Central PMCID: PMC5076890.
7. Benda J. Neural adaptation. Curr Biol. 2021;31(3):R110-R6. doi: 10.1016/j.cub.2020.11.054. PubMed PMID: 33561404.
8. Verhagen JV, Wesson DW, Netoff TI, White JA, Wachowiak M. Sniffing controls an adaptive filter of sensory input to the olfactory bulb. Nat Neurosci. 2007;10(5):631-9. doi: 10.1038/nn1892. PubMed PMID: 17450136.
9. Gottfried JA. Central mechanisms of odour object perception. Nat Rev Neurosci. 2010;11(9):628-41. doi: 10.1038/nrn2883. PubMed PMID: 20700142; PubMed Central PMCID: PMC3722866.
10. Martelli C, Storace DA. Stimulus Driven Functional Transformations in the Early Olfactory System. Frontiers in Cellular Neuroscience. 2021;15(288). doi: 10.3389/fncel.2021.684742.

901 11. Rokni D, Hemmelder V, Kapoor V, Murthy VN. An olfactory cocktail party: figure-ground segregation of
902 odorants in rodents. Nat Neurosci. 2014;17(9):1225-32. doi: 10.1038/nn.3775. PubMed PMID: 25086608;
903 PubMed Central PMCID: PMC4146660.
904 12. Duchamp-Viret P, Chaput MA, Duchamp A. Odor response properties of rat olfactory receptor neurons.
905 Science. 1999;284(5423):2171-4. Epub 1999/06/26. doi: 7612 [pii]. PubMed PMID: 10381881.
906 13. Ma M, Shepherd GM. Functional mosaic organization of mouse olfactory receptor neurons. Proc Natl
907 Acad Sci U S A. 2000;97(23):12869-74. doi: 10.1073/pnas.220301797. PubMed PMID: 11050155; PubMed
908 Central PMCID: PMC18856.
909 14. Zak JD, Reddy G, Vergassola M, Murthy VN. Antagonistic odor interactions in olfactory sensory
910 neurons are widespread in freely breathing mice. Nat Commun. 2020;11(1):3350. doi: 10.1038/s41467-020-
911 17124-5. PubMed PMID: 32620767; PubMed Central PMCID: PMC7335155.
912 15. Storace DA, Cohen LB. Measuring the olfactory bulb input-output transformation reveals a contribution
913 to the perception of odorant concentration invariance. Nat Commun. 2017;8(1):81. Epub 2017/07/21. doi:
914 10.1038/s41467-017-00036-2. PubMed PMID: 28724907; PubMed Central PMCID: PMCPMC5517565.
915 16. Wachowiak M, Cohen LB. Representation of odorants by receptor neuron input to the mouse olfactory
916 bulb. Neuron. 2001;32(4):723-35. Epub 2001/11/24. doi: S0896-6273(01)00506-2 [pii]. PubMed PMID:
917 11719211.
918 17. Fried HU, Fuss SH, Korsching SI. Selective imaging of presynaptic activity in the mouse olfactory bulb
919 shows concentration and structure dependence of odor responses in identified glomeruli. Proc Natl Acad Sci U
920 S A. 2002;99(5):3222-7. Epub 2002/02/21. doi: 10.1073/pnas.052658399 052658399 [pii]. PubMed PMID:
921 11854464.
922 18. Mombaerts P, Wang F, Dulac C, Chao SK, Nemes A, Mendelsohn M, et al. Visualizing an olfactory
923 sensory map. Cell. 1996;87(4):675-86. Epub 1996/11/15. doi: S0092-8674(00)81387-2 [pii]. PubMed PMID:
924 8929536.
925 19. Potter SM, Zheng C, Koos DS, Feinstein P, Fraser SE, Mombaerts P. Structure and emergence of
926 specific olfactory glomeruli in the mouse. J Neurosci. 2001;21(24):9713-23. PubMed PMID: 11739580;
927 PubMed Central PMCID: PMC2570017.

928 20. Igarashi KM, Ieki N, An M, Yamaguchi Y, Nagayama S, Kobayakawa K, et al. Parallel mitral and tufted
929 cell pathways route distinct odor information to different targets in the olfactory cortex. J Neurosci.
930 2012;32(23):7970-85. doi: 10.1523/jneurosci.0154-12.2012. PubMed PMID: 22674272; PubMed Central
931 PMCID: PMC3636718.
932 21. Storace DA, Cohen LB, Choi Y. Using Genetically Encoded Voltage Indicators (GEVIs) to Study the
933 Input-Output Transformation of the Mammalian Olfactory Bulb. Front Cell Neurosci. 2019;13:342. Epub
934 2019/08/17. doi: 10.3389/fncel.2019.00342. PubMed PMID: 31417362; PubMed Central PMCID:
935 PMCPMC6684792.
936 22. Storace DA, Cohen LB. The mammalian olfactory bulb contributes to the adaptation of odor responses:
937 a second perceptual computation carried out by the bulb. eNeuro. 2021. Epub 20210811. doi:
938 10.1523/ENEURO.0322-21.2021. PubMed PMID: 34380657.
939 23. Kato HK, Chu MW, Isaacson JS, Komiyama T. Dynamic sensory representations in the olfactory bulb:
940 modulation by wakefulness and experience. Neuron. 2012;76(5):962-75. doi: 10.1016/j.neuron.2012.09.037.
941 PubMed PMID: 23217744; PubMed Central PMCID: PMC3523713.
942 24. Ogg MC, Bendahamane M, Fletcher ML. Habituation of glomerular responses in the olfactory bulb
943 following prolonged odor stimulation reflects reduced peripheral input. Front Mol Neurosci. 2015;8:53. doi:
944 10.3389/fnmol.2015.00053. PubMed PMID: 26441516; PubMed Central PMCID: PMC4585128.
945 25. Ogg MC, Ross JM, Bendahmane M, Fletcher ML. Olfactory bulb acetylcholine release dishabituates
946 odor responses and reinstates odor investigation. Nat Commun. 2018;9(1):1868. doi: 10.1038/s41467-018-
947 04371-w. PubMed PMID: 29760390; PubMed Central PMCID: PMC5951802.
948 26. Mitsui S, Igarashi KM, Mori K, Yoshihara Y. Genetic visualization of the secondary olfactory pathway in
949 Tbx21 transgenic mice. Neural Syst Circuits. 2011;1(1):5. doi: 10.1186/2042-1001-1-5. PubMed PMID:
950 22330144; PubMed Central PMCID: PMC3257540.
951 27. Daigle TL, Madisen L, Hage TA, Valley MT, Knoblich U, Larsen RS, et al. A Suite of Transgenic Driver
952 and Reporter Mouse Lines with Enhanced Brain-Cell-Type Targeting and Functionality. Cell. 2018;174(2):465-
953 80 e22. doi: 10.1016/j.cell.2018.06.035. PubMed PMID: 30007418; PubMed Central PMCID: PMC6086366.
954 28. Rinberg D, Koulakov A, Gelperin A. Sparse odor coding in awake behaving mice. J Neurosci.
955 2006;26(34):8857-65. doi: 10.1523/jneurosci.0884-06.2006. PubMed PMID: 16928875.

956 29. Wachowiak M, Economo MN, Diaz-Quesada M, Brunert D, Wesson DW, White JA, et al. Optical
957 dissection of odor information processing in vivo using GCaMPs expressed in specified cell types of the
958 olfactory bulb. J Neurosci. 2013;33(12):5285-300. doi: 10.1523/jneurosci.4824-12.2013. PubMed PMID:
959 23516293; PubMed Central PMCID: PMC3690468.
960 30. Wesson DW, Carey RM, Verhagen JV, Wachowiak M. Rapid encoding and perception of novel odors in
961 the rat. PLoS Biol. 2008;6(4):e82. doi: 10.1371/journal.pbio.0060082. PubMed PMID: 18399719; PubMed
962 Central PMCID: PMC2288628.
963 31. Huang JS, Kunkhyen T, Rangel AN, Brechbill TR, Gregory JD, Winson-Bushby ED, et al. Immature
964 olfactory sensory neurons provide behaviourally relevant sensory input to the olfactory bulb. Nat Commun.
965 2022;13(1):6194. Epub 20221019. doi: 10.1038/s41467-022-33967-6. PubMed PMID: 36261441; PubMed
966 Central PMCID: PMCPMC9582225.
967 32. Margrie TW, Sakmann B, Urban NN. Action potential propagation in mitral cell lateral dendrites is
968 decremental and controls recurrent and lateral inhibition in the mammalian olfactory bulb. Proc Natl Acad Sci U
969 S A. 2001;98(1):319-24. doi: 10.1073/pnas.011523098. PubMed PMID: 11120888; PubMed Central PMCID:
970 PMC14588.
971 33. Wilson DA. Habituation of odor responses in the rat anterior piriform cortex. J Neurophysiol.
972 1998;79(3):1425-40. doi: 10.1152/jn.1998.79.3.1425. PubMed PMID: 9497422.
973 34. Kadohisa M, Wilson DA. Olfactory cortical adaptation facilitates detection of odors against background.
974 J Neurophysiol. 2006;95(3):1888-96. doi: 10.1152/jn.00812.2005. PubMed PMID: 16251260; PubMed Central
975 PMCID: PMC2292127.
976 35. Sobel EC, Tank DW. Timing of odor stimulation does not alter patterning of olfactory bulb unit activity in
977 freely breathing rats. J Neurophysiol. 1993;69(4):1331-7. Epub 1993/04/01. PubMed PMID: 8492167.
978 36. Carey RM, Verhagen JV, Wesson DW, Pirez N, Wachowiak M. Temporal structure of receptor neuron
979 input to the olfactory bulb imaged in behaving rats. J Neurophysiol. 2009;101(2):1073-88. doi:
980 10.1152/jn.90902.2008. PubMed PMID: 19091924; PubMed Central PMCID: PMC2657066.
981 37. Lecoq J, Tiret P, Charpak S. Peripheral adaptation codes for high odor concentration in glomeruli. J
982 Neurosci. 2009;29(10):3067-72. doi: 10.1523/jneurosci.6187-08.2009. PubMed PMID: 19279243.

983 38. Wesson DW, Donahou TN, Johnson MO, Wachowiak M. Sniffing behavior of mice during performance
984 in odor-guided tasks. Chem Senses. 2008;33(7):581-96. Epub 20080605. doi: 10.1093/chemse/bjn029.
985 PubMed PMID: 18534995; PubMed Central PMCID: PMCPMC2533419.
986 39. Platisa J, Zeng H, Madisen L, Cohen LB, Pieribone VA, Storace DA. Voltage imaging in the olfactory
987 bulb using transgenic mouse lines expressing the genetically encoded voltage indicator ArcLight. Sci Rep.
988 2022;12(1):1875. Epub 20220203. doi: 10.1038/s41598-021-04482-3. PubMed PMID: 35115567; PubMed
989 Central PMCID: PMCPMC8813909.
990 40. Chu MW, Li WL, Komiyama T. Lack of Pattern Separation in Sensory Inputs to the Olfactory Bulb during
991 Perceptual Learning. eNeuro. 2017;4(5). doi: 10.1523/eneuro.0287-17.2017. PubMed PMID: 28955724;
992 PubMed Central PMCID: PMC5615249.
993 41. Eiting TP, Wachowiak M. Differential Impacts of Repeated Sampling on Odor Representations by
994 Genetically-Defined Mitral and Tufted Cell Subpopulations in the Mouse Olfactory Bulb. J Neurosci.
995 2020;40(32):6177-88. doi: 10.1523/jneurosci.0258-20.2020. PubMed PMID: 32601245; PubMed Central
996 PMCID: PMC7406285.
997 42. Kikuta S, Fletcher ML, Homma R, Yamasoba T, Nagayama S. Odorant response properties of individual
998 neurons in an olfactory glomerular module. Neuron. 2013;77(6):1122-35. doi: 10.1016/j.neuron.2013.01.022.
999 PubMed PMID: 23522047; PubMed Central PMCID: PMC3607817.
1000 43. Dhawale AK, Hagiwara A, Bhalla US, Murthy VN, Albeanu DF. Non-redundant odor coding by sister
1001 mitral cells revealed by light addressable glomeruli in the mouse. Nat Neurosci. 2010;13(11):1404-12. doi:
1002 10.1038/nn.2673. PubMed PMID: 20953197; PubMed Central PMCID: PMC3208311.
1003 44. Nagayama S, Zeng S, Xiong W, Fletcher ML, Masurkar AV, Davis DJ, et al. In vivo simultaneous tracing
1004 and Ca(2+) imaging of local neuronal circuits. Neuron. 2007;53(6):789-803. Epub 2007/03/16. doi: S0896-
1005 6273(07)00138-9 [pii] 10.1016/j.neuron.2007.02.018. PubMed PMID: 17359915.
1006 45. Djurisic M, Antic S, Chen WR, Zecevic D. Voltage imaging from dendrites of mitral cells: EPSP
1007 attenuation and spike trigger zones. J Neurosci. 2004;24(30):6703-14. Epub 2004/07/30. doi:
1008 10.1523/JNEUROSCI.0307-04.2004 24/30/6703 [pii]. PubMed PMID: 15282273.

1009 46. Charpak S, Mertz J, Beaurepaire E, Moreaux L, Delaney K. Odor-evoked calcium signals in dendrites
1010 of rat mitral cells. Proc Natl Acad Sci U S A. 2001;98(3):1230-4. doi: 10.1073/pnas.021422798. PubMed PMID:
1011 11158622; PubMed Central PMCID: PMC14737.
1012 47. Leong LM, Storace DA. Imaging different cell populations in the mouse olfactory bulb using the
1013 genetically encoded voltage indicator ArcLight. Neurophotonics. 2024;11(3):033402. Epub 20240117. doi:
1014 10.1117/1.NPh.11.3.033402. PubMed PMID: 38288247; PubMed Central PMCID: PMCPMC10823906.
1015 48. Dietz SB, Murthy VN. Contrasting short-term plasticity at two sides of the mitral-granule reciprocal
1016 synapse in the mammalian olfactory bulb. J Physiol. 2005;569(Pt 2):475-88. doi:
1017 10.1113/jphysiol.2005.095844. PubMed PMID: 16166156; PubMed Central PMCID: PMC1464232.
1018 49. Chaudhury D, Manella L, Arellanos A, Escanilla O, Cleland TA, Linster C. Olfactory bulb habituation to
1019 odor stimuli. Behav Neurosci. 2010;124(4):490-9. doi: 10.1037/a0020293. PubMed PMID: 20695648; PubMed
1020 Central PMCID: PMC2919830.
1021 50. Banerjee A, Marbach F, Anselmi F, Koh MS, Davis MB, Garcia da Silva P, et al. An Interglomerular
1022 Circuit Gates Glomerular Output and Implements Gain Control in the Mouse Olfactory Bulb. Neuron.
1023 2015;87(1):193-207. doi: 10.1016/j.neuron.2015.06.019. PubMed PMID: 26139373; PubMed Central PMCID:
1024 PMC4633092.
1025 51. Fantana AL, Soucy ER, Meister M. Rat olfactory bulb mitral cells receive sparse glomerular inputs.
1026 Neuron. 2008;59(5):802-14. Epub 2008/09/13. doi: S0896-6273(08)00678-8 [pii]
1027 10.1016/j.neuron.2008.07.039. PubMed PMID: 18786363.
1028 52. Braubach O, Tombaz T, Geiller T, Homma R, Bozza T, Cohen LB, et al. Sparsened neuronal activity in
1029 an optogenetically activated olfactory glomerulus. Sci Rep. 2018;8(1):14955. doi: 10.1038/s41598-018-33021-
1030 w. PubMed PMID: 30297851; PubMed Central PMCID: PMC6175855.
1031 53. Short SM, Wachowiak M. Temporal Dynamics of Inhalation-Linked Activity across Defined
1032 Subpopulations of Mouse Olfactory Bulb Neurons Imaged In Vivo. eNeuro. 2019;6(3). doi:
1033 10.1523/eneuro.0189-19.2019. PubMed PMID: 31209151; PubMed Central PMCID: PMC6597857.
1034 54. Parabucki A, Bizer A, Morris G, Munoz AE, Bala ADS, Smear M, et al. Odor Concentration Change
1035 Coding in the Olfactory Bulb. eNeuro. 2019;6(1). doi: 10.1523/eneuro.0396-18.2019. PubMed PMID:
1036 30834303; PubMed Central PMCID: PMC6397952.

1037 55. Williams E, Dewan A. Olfactory Detection Thresholds for Primary Aliphatic Alcohols in Mice. Chem
1038 Senses. 2020;45(7):513-21. doi: 10.1093/chemse/bjaa045. PubMed PMID: 32609815; PubMed Central
1039 PMCID: PMCPMC7750973.

1040

1041